IOP Publishing Superconductor Science and Technology
Supercond. Sci. Technol. **36** (2023) 035005 (9pp) https://doi.org/10.1088/1361-6668/acb10e

An RF SQUID readout for a flux qubit-based microwave single photon counter

V I Shnyrkov[1,2], A P Shapovalov[1,2], V Yu Lyakhno[1,3,*], A O Dumik[1], A A Kalenyuk[1] and P Febvre[4]

[1] Department of Superconductivity, G.V. Kurdyumov Institute for Metal Physics of the N.A.S. of Ukraine, Kyiv, Ukraine
[2] Research Center for Quantum Materials and Quantum Technologies, Kyiv Academic University of the N.A.S. and M.E.S. of Ukraine, Kyiv, Ukraine
[3] Department of Superconductive and Mesoscopic Structures, B.I. Verkin Institute for Low Temperature Physics and Engineering of the N.A.S. of Ukraine, Kharkiv, Ukraine
[4] IMEP-LAHC, Université Savoie Mont Blanc, Le Bourget du Lac, France

E-mail: lyakhno@ilt.kharkov.ua

Received 20 September 2022, revised 16 December 2022
Accepted for publication 5 January 2023
Published 24 January 2023

Abstract

An analysis of the measurement of the magnetic flux in superconducting qubits based on RF SQUIDs was carried out with an 800 MHz bandwidth low-power-consumption cryogenic high-electron-mobility transistor amplifier. The preliminary experimental results obtained at temperatures 2 K and 4 K for RF SQUIDs in hysteretic, and in two non-hysteretic, regimes with a pump frequency of about 30 MHz are discussed. Parameters of RF SQUIDs in the hysteretic and non-hysteretic modes are analyzed within the framework of the resistively and capacitively shunted junction model for Josephson junctions. Its sensitivity at a temperature of 30 mK and frequency band (speed) are calculated and optimized to read the states of a flux qubit used as a single microwave photon counter. It is shown that an RF SQUID, operated in an adiabatic non-hysteretic mode for qubit readout, allows us to minimize its back-action effect and the dark count rate. This is due to the absence of Josephson generation, the small amplitude of the resonator electromagnetic field, and the selection of the pump frequency that does not coincide with the characteristic frequencies of the flux qubit.

Keywords: quantum measurements, Josephson junction, flux qubit, DC/RF SQUID, cryogenic HEMT amplifier, parametric up converter

(Some figures may appear in colour only in the online journal)

1. Introduction

Superconducting qubits are macroscopic quantum objects (artificial atoms), which form the basis for building microwave (MW) quantum photonics and quantum information devices. The MW single photon counter [1, 2] is a key element for a range of prospective quantum technologies and applications [3]. For example, the reliability of quantum cryptography protocols is based on the assumption that the secret code (key) is distributed by single photons [4]. The generation of single photons in the MW range using superconducting qubits has already been achieved [5, 6]. The first single MW photon counter [1] was created on the basis of a Josephson junction with discrete energy levels and exploited MW-photon induced transitions between them. For obvious reasons, it had a large

* Author to whom any correspondence should be addressed.

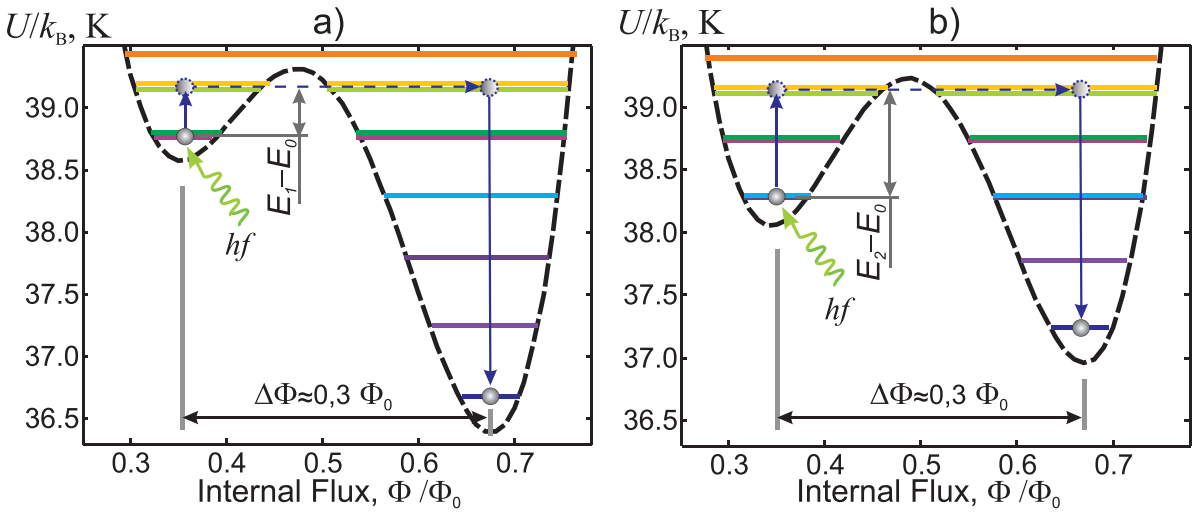

Figure 1. Potential and energy levels of flux qubit in a two-well potential of the photon counter. (a) The counter is installed in the left well by an external magnetic flux pulse $\Phi_e = 0.5052 \cdot \Phi_0$. The distance between the ground and excited states of the qubit is $\Delta T_{01} = (E_1 - E_0)/k_B \cong 0.4\,\mathrm{K}$ ($f \approx 8.2\,\mathrm{GHz}$). (b) The counter is installed to create a system of three levels at the point $\Phi_e = 0.5026 \cdot \Phi_0$ with spacing $\Delta T_{02} = (E_2 - E_0)/k_B \cong 0.83\,\mathrm{K}$ ($f \approx 17.4\,\mathrm{GHz}$).

dead time. This is the Joule heating of the Josephson junction after it has absorbed MW photons and switched out of the zero-voltage state to the voltage state. The junction cools down to the equilibrium temperature with a thermal time constant, which is long at low temperature $T \sim 10\,\mathrm{mK}$. One possible way to resolve this issue is to use the RF SQUID configuration loop (flux qubit with discrete nondegenerate spacing energy levels) as a sensitive element of the MW single-photon counter. In this case, the technique is analogous to the current pulses installation of a Josephson junction counter [1], but for a flux qubit, the tunneling process leads to a change in the magnetic flux with a short thermal time constant. Rapid continuous measurement of the final states of a qubit with minimum back-action effect (and minimum number of dark counts) of the classical readout device is a crucial experimental issue in the area of MW quantum physics.

Figure 1 schematically shows the initial (the left well) and final (the right well) states of the flux qubit after it has absorbed an incident MW photon in the MW single photon counter [7]. The potential energy and energy levels of the flux qubit are tuned to absorb MW single photons from the incident field. The MW resonant photon $h \cdot f \cong E_1 - E_0$ induces transition from the lower energy level E_0 (initial state) to the upper level E_1, for which the potential barrier separating the two classical wells is smaller, so that qubit state tunnels from the 'left' well to the 'right' one (final state). For the upper level E_1 the tunneling rate increases by a factor of approximately 10^3. The potential and energy levels are calculated by solving the Schrödinger equation (by the method described in detail in the work [8]) with the following parameters: qubit inductance $L_q = 240\,\mathrm{pH}$, critical current of the Josephson junction $I_c = 2.01\,\mu\mathrm{A}$, SIS junction capacitance $C = 0.32\,\mathrm{pF}$, and dimensionless parameter $\beta_L = 2\pi \cdot L_q \cdot I_c/\Phi_0 = 1.3$ shown in figure 1.

It can be seen from figure 1 that after tunneling from the 'left' well to the 'right' one (final state) the magnetic flux in the qubit changes by $\Delta\Phi \approx 0.3 \cdot \Phi_0$, where $\Phi_0 = h/2e \approx 2.07 \times 10^{-15}\,\mathrm{Wb}$ is the quantum of magnetic flux. Broadband flux noise associated with the shunt resistor ($\sim$10 Ohm) of the RF SQUID readout has the backaction effect on the qubit and can lead to unwanted transitions, i.e. increase the number of dark counts. One solution to this problem is to reduce this effect by weak coupling the RF SQUID to the flux qubit, as in the weak continuous measurement (WCM) method. Therefore, the circuit is designed so that only a small fraction of this flux change ($\sim 0.01 \cdot \Phi_0$) is transmitted to the RF SQUID by inductive coupling. For such a method, the signal at the SQUID input will have a value approximately equal to $\delta\Phi \approx 3 \times 10^{-3}\Phi_0\sqrt{\mathrm{Hz}}^{-1}$, where $\delta\Phi$, in other words, is the minimum resolvable value of the magnetic flux variations in the frequency band.

Two basic requirements should be met to obtain discrete energy levels in the potential wells of the qubit: (a) the intrinsic temperature of the qubit must be reduced to $T \leqslant (E_1 - E_0)/20k_B \sim 20\,\mathrm{mK}$ to suppress the effect of level mixing by thermal fluctuations. Careful electrical filtering and magnetic shielding can eliminate excess temperature due to environmental noise. (b) The broadening of energy levels due to dissipation should be small. The resistance introduced by the control and readout circuits that can be ascribed to an equivalent resistor shunting the Josephson junction of the qubit should be $R_\Sigma \geqslant 10\,\mathrm{kOhm}$.

In principle, such a change in the magnetic flux in the qubit $\Delta\Phi \approx 0.3 \cdot \Phi_0$ can be measured in a relatively short time using direct current SQUID (DC SQUID), which has a magnetic flux noise of $\delta\Phi \approx 10^{-7}\Phi_0/\sqrt{\mathrm{Hz}}$, and energy sensitivity of $\delta\varepsilon_V = \delta\Phi^2/2L \approx 10^{-33}\,\mathrm{J\,Hz^{-1}}$ [9, 10]. The DC SQUID can be considered as a parametric detector with internal pumping at the Josephson frequency $\omega_J/2\pi$, ($2eV = \hbar\omega_J$). To obtain the sensitivity of the DC SQUID at this level, the operating point should be set at a high voltage V, at which the electromagnetic fields of Josephson oscillations with frequencies of 30–100 GHz directly affect the measured quantum system. In a

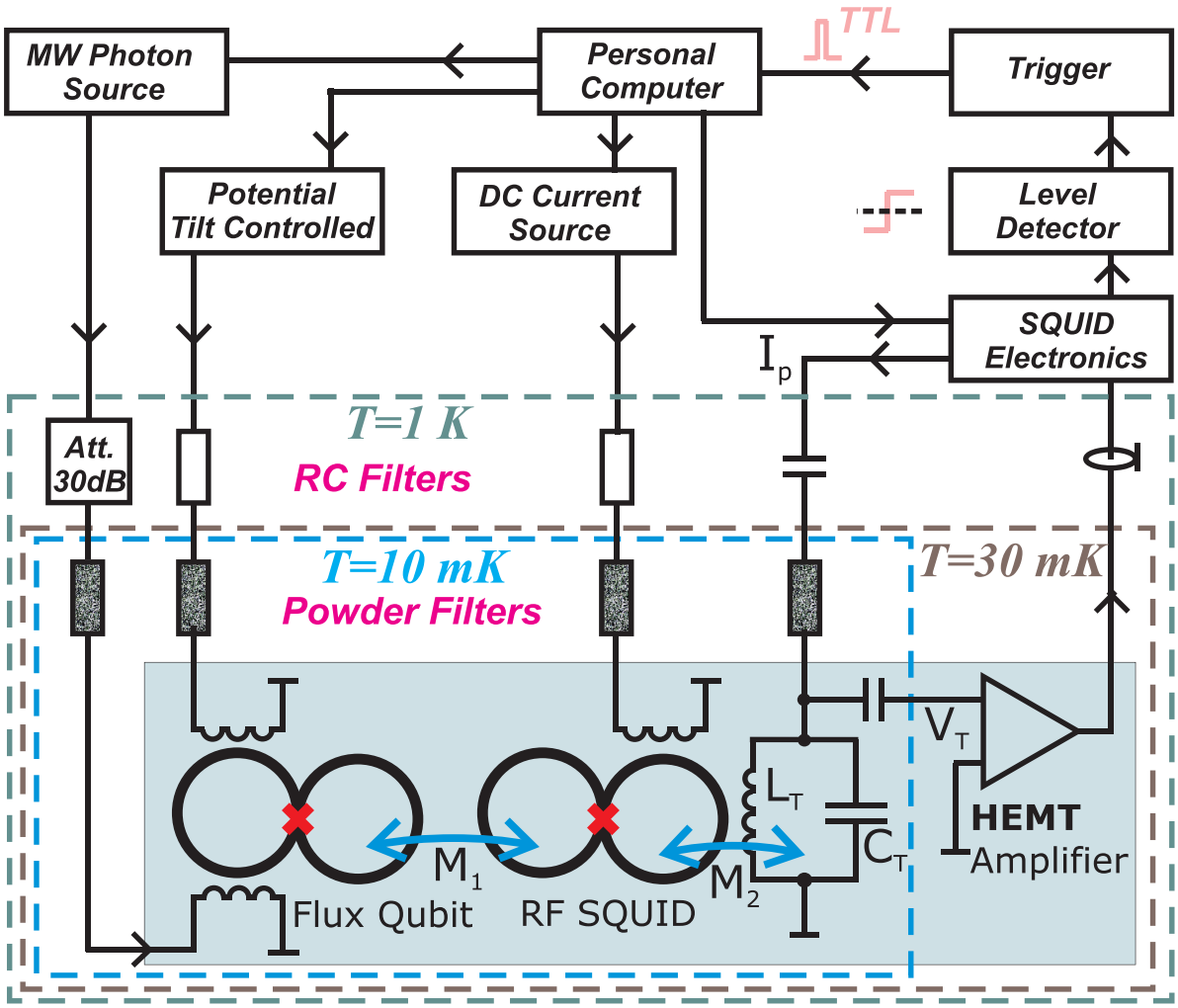

Figure 2. Schematic circuit diagram for recording a photon-induced transition in the flux qubit. The readout circuit based on RF SQUID with Josephson junction critical current I_C, capacitance C, and shunt resistance R. Oscillations in the resonator $L_T \cdot C_T$, with quality factor Q, inductively coupled M_2 to the interferometer, are excited by the current of the external generator $I_P = I_{PO}\cos(\Omega_P \cdot t + \theta)$ and are amplified by a HEMT amplifier based on AVAGO ATF36077 operating in unsaturated mode. The excitation frequency $\Omega_P/2\pi \approx 0.5$ GHz is selected from the condition $(E_1 - E_0)/\hbar \gg \Omega_P$. A change in the magnetic flux in a qubit (after absorption of a photon) induces a change in the flux (M_1 signal) in an RF SQUID.

MW single photon counter, Josephson oscillations and broadband noise from shunt resistors of the DC SQUID readout will lead to unwanted state transitions and to an increase in the number of dark counts. These effects can be suppressed by reducing the coupling between the flux qubit and the DC SQUID, proportionally decreasing the signal amplitude [11]. Despite these drawbacks, only DC SQUIDs are currently used to measure the flux qubit states by the method of WCM. Note that since the time of appearance of a photon is unknown, other measurement techniques, for example, with switching 'on' and 'off' of DC SQUIDS, are extremely inconvenient in this case.

In an RF SQUID, a Josephson junction with a critical current I_c, and a normal resistance R, is shunted by a superconducting circuit with a geometric inductance L. Since there is no Josephson generation in RF SQUIDs, and one can choose the pump frequency to be much lower than the characteristic frequency of the MW photon, using RF SQUIDs for the readout can reduce the number of dark counts. Another important parameter, the amplitude of the electromagnetic pumping field in the resonator, depends on the mode of operation of the RF SQUID and will be discussed below.

To register signals in RF SQUIDs, a basic tank circuit is used (figure 2) with 'external' pumping current $I_P = I_{PO} \cdot \cos(\Omega_P \cdot t + \theta)$ from a generator at frequency $\Omega_P/2\pi$ close to the natural frequency $\omega_T/2\pi = 1/(2\pi \cdot \sqrt{L_T \cdot C_T})$ of the resonator, detuning $\xi_0 = (\Omega_P - \omega_T)/\omega_T \ll 1$ and quality factor $Q \gg 1$ [10, 12]. The normalized external variable magnetic flux $a = 2\pi \cdot \Phi_a/\Phi_0$ is set in the SQUID interferometer via inductive coupling $M_2 = k\sqrt{L \cdot L_T}$ with the resonator so that the condition $k^2 \cdot Q \approx 1$ is satisfied.

The first stage of the high-electron-mobility transistor (HEMT) amplifier with low DC power consumption ($P_{DC} \approx 3\,\mu$W) at ultralow supply voltages in the unsaturated region of the static characteristic [13] and low brightness temperature [14] should be located at a temperature zone of the refrigerator

with $T \approx 30$ mK [15]. A cryogenic amplifier placed at 30 mK allows us to reduce the intrinsic noise of the resonator and improve the sensitivity of the RF SQUID. Furthermore, the HEMT AVAGO ATF36077 has a low gate leakage current and a high mechanical stability during multiple thermal cycling. All the above makes ATF36077 a suitable HEMT in the considered WCM method. A photon-induced transition is recorded by the RF SQUID magnetometer and sent to the level detector to send a trigger pulse to the computer, which records this event and generates a signal for the next installation of the flux qubit through the 'potential tilt controlled' block.

A change in the signal, at the input of the RF SQUID due to the mutual inductance M_1, leads to variations in the voltage, frequency, and phase of the oscillations in the tank resonator. The magnetic flux-to-voltage (or phase) transfer coefficients, sensitivity and back-action effects on the measured device depend on many parameters and will be discussed below. Let us now turn to the analysis of RF SQUIDs for measuring the states of a flux qubit in the MW single photon counter, which is a quantum object with discrete energy levels, as shown in figure 1.

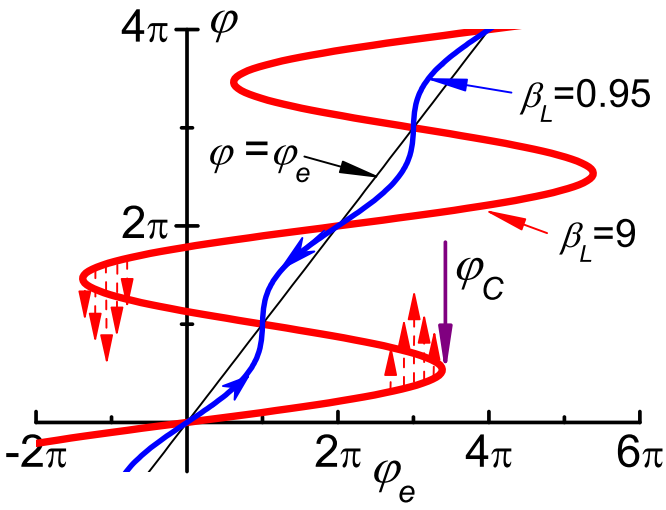

Figure 3. Dependence of the phase difference of the Josephson junction φ on the normalized external magnetic flux φ_e in the RF SQUID loop with $\beta_L = 9$ and $\beta_L = 0.95$. Arrows show the regions of phase jumps while sweeping the external flux with the RF generator $\varphi_e \propto \sin(\Omega_P \cdot t + \theta)$.

2. RF SQUID in hysteretic mode $\beta_L > 1$

The magnetic flux in the RF SQUID loop Φ is directly related to the phase difference φ at the junction and consequently to the effective inductance of the Josephson junction L_J (Josephson inductance)

$$\varphi = 2\pi \cdot \frac{\Phi}{\Phi_0}, \qquad L_J = \frac{\Phi_0}{2\pi \cdot I_c \cos(\varphi)}. \tag{1}$$

Therefore, any variations in the external magnetic flux in the RF SQUID causes a change in the total reactive impedance of the interferometer. In the hysteretic mode [5, 7], the parameter $\beta_L = 2\pi \cdot L \cdot I_c/\Phi_0 > 1$ and, with a slow sweep of the external flux $\varphi_e(t)$ with respect to the switching time of the interferometer $\Omega_P \ll R/L$, the dependence of φ on the normalized external flux $\varphi_e = 2\pi\Phi_e/\Phi_0$ following from the stationary equation is multi-valued.

$$\beta_L \cdot \sin(\varphi) + \varphi = \varphi_e \tag{2}$$

The presence of areas of ambiguity in the function $\varphi(\varphi_e)$ is the main distinguishing feature of the hysteretic mode, and the branches with $d\varphi/d\varphi_e < 0$ are unstable, which leads to jumps from one stable state to another one and to a hysteresis in the $\varphi(\varphi_e)$ curve. Phase jumps and hysteretic losses occur when the oscillation amplitude reaches the region near the critical phase value $\varphi_e \approx \varphi_c$ (figure 3) proportional to β_L, for which the screening current in the RF SQUID reaches the critical current of the junction.

The energy dissipated in the junction during the jump of the hysteretic curve is taken from the resonant circuit. This additional dissipation leads to the appearance of almost horizontal steps in the high-frequency current–voltage $(I - V)$ and amplitude-frequency characteristics (AFC) of RF SQUIDs. Examples of such almost horizontal steps are shown in figure 4. It is important to note that the RF SQUID in the hysteretic mode operates mainly as a nonlinear active element, although the root cause of the hysteresis losses is its nonlinear inductance L_J given by equation (1).

This regime has been well studied [10, 12] and is widely used in various classical experiments. The magnetic flux-to-voltage transfer coefficient of the RF SQUID in the hysteretic mode $\eta_a = dV_T/d\Phi_e$ does not depend on the superconducting properties of the junction.

$$\eta_a = \frac{\Omega_P}{k} \cdot \sqrt{\frac{L_T}{L}} = \frac{1}{M_2 \cdot \Omega_P \cdot C_T} \tag{3}$$

In the normal case, when the main source of noise is the amplifier V_{NA}, the transfer coefficient η_a determines the sensitivity of the RF SQUID in the frequency band Δf

$$\delta\varepsilon = \delta\varepsilon_A = \frac{\langle \delta\Phi_{NA} \rangle^2}{2L \cdot \Delta f} = \frac{1}{2L} \cdot \frac{\langle V_{NA} \rangle^2}{|\eta_a|^2 \cdot \Delta f}; \qquad \delta\varepsilon_A \sim \left(\frac{k}{\Omega_P}\right)^2, \tag{4}$$

where the $\delta\varepsilon$ is the ultimate sensitivity of the SQUID in terms of energy.

When measuring weak signals from quantum objects without using feedback, the sensitivity can be improved, see equations (3) and (4), by slightly reducing the coupling coefficient k and abandoning the triangular signal characteristic, which requires the condition $k^2 \cdot Q \approx 1$ to be met. However, the main ways to improve the sensitivity are to increase the pump frequency Ω_P and reduce the amplifier noise (equations (3) and (4)). It is the increase in Ω_P, as well as the decrease in the noise of cooled amplifiers, that made it possible to approach the RF SQUIDs sensitivity limited only by the noise in the Josephson junction [16, 17]. The uncertainty of the oscillation amplitude at the time of the jump due to

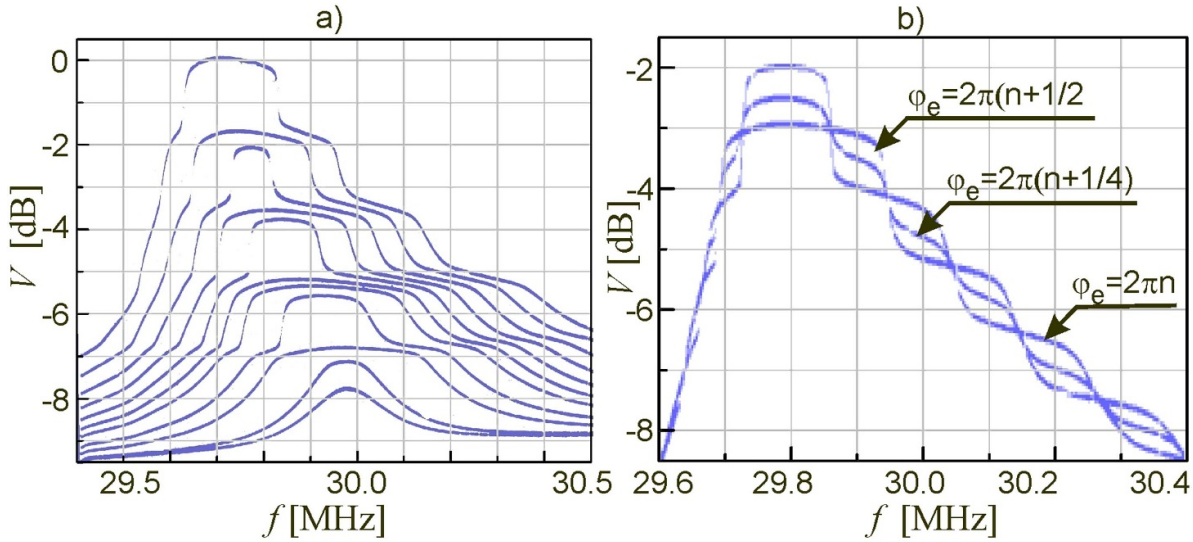

Figure 4. Sets of amplitude-frequency characteristics of RF SQUID in hysteretic regime measured at pumping frequency ∼30 MHz at a temperature of $T = 4.2$ K in a frequency band of 15 kHz. (a) The resonator pumping amplitude changes by 1 dB per curve at a constant value of external magnetic flux $\varphi_e = 2\pi \cdot n$ for all. In the region of low excitation amplitudes, the resonator is linear and there are no horizontal steps or signal characteristics. (b) AFC for three values φ_e at constant excitation amplitude.

thermal fluctuations is a source of internal noise in the hysteretic regime of the RF SQUID. In figure 3 this specific sensor noise area is indicated by dotted arrows. The width $\Delta\sigma$ of the probability density distribution of the jumps depends on the temperature, $\Delta\sigma \sim T^{2/3}$ [13], and causes a finite slope of the steps in the RF current–voltage characteristics of the SQUID. This slope originates from another noise 'at the output' of the RF SQUID, namely, the thermal fluctuations in the resonator. A numerical analysis of the RF SQUID sensitivity, taking into account the noise of the interferometer, resonator, and amplifier, was performed in [18]. This analysis is based on the average slope of the step $\mathcal{L}_{\rm JB} \sim \Delta\sigma \sim T^{2/3}$, introduced by the authors, which is assumed to be constant along the step length. The parameter $\mathcal{L}_{\rm JB}$ was used in almost all subsequent works when optimizing the sensitivity of RF SQUIDs with $\beta_{\rm L} > 1$. Analysis of the fine structure of the step [12, 19] shows that there is a single minimum of local curvature on the step, which determines the penetration of the resonator noise 'to the output' (figure 5). Calculations of the RF SQUID sensitivity using the $\mathcal{L}_{\rm JB}$ parameter give slightly worse figures as compared to the real device.

In the diagram shown in figure 2, the temperature $T_{\rm T}$ of the resonator is approximately equal to the temperature of the interferometer, $T_{\rm T} \approx T$. The ratio of the noise intensities of the resonator and the RF SQUID operating in its hysteretic mode has the form [19,20]

$$\frac{(\varepsilon_{\rm V})_{\rm T}}{(\varepsilon_{\rm V})_{\rm min}} \approx \frac{1}{2\pi \cdot k^2 \cdot Q} \cdot \frac{L}{L_{\rm F}} \cdot \frac{T_{\rm T}}{T}, \qquad L_{\rm F} = \frac{(\Phi_0)^2}{(2\pi)^2 \cdot k_{\rm B} \cdot T} \quad (5)$$

Since $k^2 \cdot Q \approx 1$ and $L/L_{\rm F} \ll 1$ the contribution of the resonator noise to the RF SQUID sensitivity is always less than the 'intrinsic' noise determined by fluctuations in the interferometer. However, when the RF SQUID with

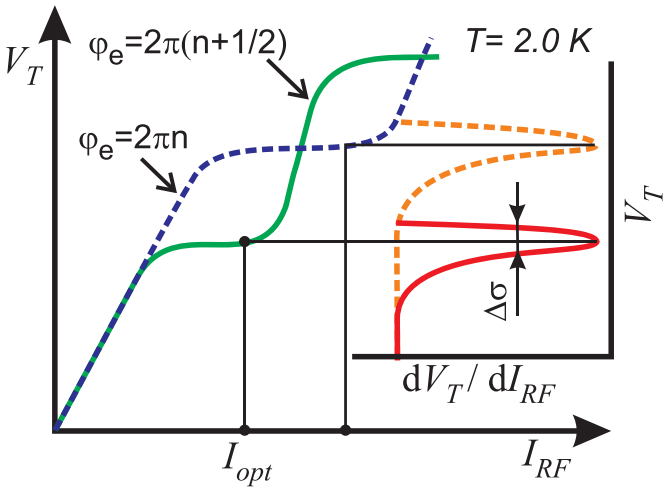

Figure 5. $I - V$ characteristics of the RF SQUID measured at $T \cong 2$ K for two values of the magnetic flux in hysteretic regime and the corresponding measured derivatives $dV_{\rm T}/dI_{\rm P}$ proportional to the local curvature of the steps. The characteristic value of the width $dV_{\rm T}/dI_{\rm P} \sim \mathcal{L}_{\rm JB}$ is denoted by $\Delta\sigma$. The optimal operating point for the pumping current $I_{\rm opt}$ corresponds to the minimum local curvature of the step.

parameters $\eta_a \approx 3.5 \times 10^{11}$ V Wb^{-1}, $L \approx 240$ pH, $\Omega_{\rm P}/2\pi \approx 0.5$ GHz, $k^2 \cdot Q \approx 1$, $Q \approx 300$ is cooled down to temperatures of $10 - 15$ mK, the intrinsic noise of the interferometer decreases proportionally to $\sim T^{2/3}$, and the sensitivity estimate at the optimal operating point $I_{\rm RF} = I_{\rm opt}$ (figure 5) leads to the values $\delta\varepsilon_{\rm V} \leqslant 10^{-32}$ J Hz^{-1}. Note that the back-action effect of the resonator noise 'on the input' increases if the first stage of the amplifier and part of the resonator are at temperatures $T_{\rm T} \gg T$, for example, in the temperature range 0.1–1 K. This emphasizes the importance of using a low DC power

consumption HEMT amplifier [12–14] in the signal detection circuit located at temperature ∼30 mK.

However, the operation in the hysteretic (dissipative) mode requires a sufficiently large pump current $M_2 \cdot I_{P0} \cdot Q > \Phi_C \sim I_C$ and consequently a large electromagnetic field in the resonator. Therefore, one faces the difficult problem of shielding the counter from the electromagnetic fields when measuring a photon counter signal with a hysteretic RF SQUID. By choosing the external pump frequency according to relations

$$\Omega_P \ll \frac{E_1 - E_0}{\hbar}, \qquad \Omega_P \neq \frac{E_1 - E_0}{n \cdot \hbar}, \qquad n = 1, 2, 3, \ldots \quad (6)$$

it is possible to reduce the probability of unwanted transitions in the qubit due to multiphoton absorptions [3] and therefore of the number of dark counts. However, relatively large pump amplitudes, dissipation and noise associated with the uncertainty of magnetic flux jumps make it problematic to use the hysteretic mode of RF SQUIDs in quantum measurements. The electromagnetic field acting on the qubit, the losses and the intrinsic noise of the interferometer can be radically reduced by using the RF SQUID in the non-hysteretic mode.

3. RF SQUID in the non-hysteretic regime $\beta_L < 1$

If the main parameter of the RF SQUID is less than unity $\beta_L \leqslant 1$, then there are no phase jumps and consequently no hysteresis losses, and no noise associated with the uncertainty of magnetic flux jumps. In the adiabatic non-hysteretic operation mode (determined with parameter $q = \Omega_P \cdot L/R \ll 1$) equation (2) shows that at $\beta_L \leqslant 1$ the interferometer states $\varphi(\varphi_e)$ are reversed with a change in sign of the pumping magnetic flux [12, 19, 20]. A change in the external signal causes a change of the Josephson inductance of equation (1) and of the total inductance of the interferometer coupled to the RF field of the resonator. In other words, in this case, the RF SQUID is a nonlinear reactive element in which not only the amplitude but also the frequency and phase characteristics are important. In the non-hysteretic adiabatic mode, the interferometer loop of the RF SQUID operates as an ideal parametric up-converter, and its own noises at the refrigerator temperature of 10 mK will make a negligible contribution to the sensitivity of the whole device [19, 20].

$$(\varepsilon_V)_{int} \approx \frac{k_B \cdot T}{4\beta_L \cdot f_c} \approx \frac{k_B \cdot T}{4 \cdot f_c} \quad (7)$$

Here $f_c = \omega_C/2\pi = I_c \cdot R/\Phi_0$ is the characteristic frequency of the RF SQUID Josephson junction. The intrinsic noise of the interferometer with $\beta_L < 1$ is approximately ω_C/Ω_P times less than in the hysteretic mode. In the non-hysteretic regime the RF SQUID sensitivity is limited by the resonator noise [16]

$$(\varepsilon_V)_T \approx \frac{1}{\beta_L \cdot \omega_C} \frac{k_B \cdot T_T^*}{\gamma} \quad (8)$$

where $\gamma = k^2 \cdot Q \cdot \beta_L \cdot \Omega_P/\omega_C$, and $T_T^* \approx 30$ mK is the effective resonator temperature which takes into account the noise

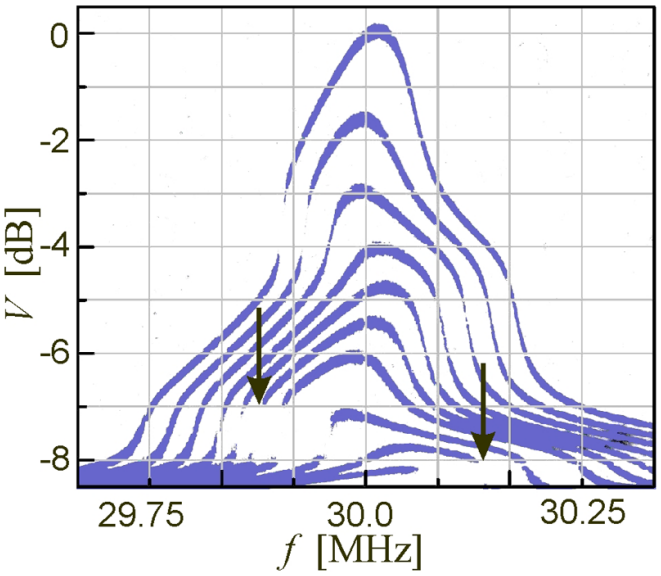

Figure 6. AFC set measured for an RF SQUID in the non-hysteretic mode with $k^2 \cdot Q \cdot \beta_L > 1$, $\beta_L \approx 0.4$ at constant external magnetic flux $\varphi_e \cong 2\pi \cdot (n + 1/2)$, $\omega_T/2\pi \cong 30$ MHz, $T \approx 4$ K. The excitation amplitude decreases by 1 dB per curve from the upper. 'Vertical' regions marked by arrows are observed both at positive and negative detuning.

impact of a two-stage ultra-low-power consumption HEMT amplifier [13, 14]. The ratio of the resonator noise of equation (8) to the interferometer noise of equation (7) is $(\varepsilon_V)_T/(\varepsilon_V)_{Int} \approx \omega_C/\Omega_P \gg 1$ and remains large. Since $k^2 \cdot Q \cdot \beta_L \leqslant 1$, then, even if the influence of the amplifier is small $T_T^* \approx T_T$. In this case, the resonator noise limits the sensitivity of the RF SQUID in the non-hysteretic mode. One can, without much error, estimate this noise from expression (7), and for $\beta_L \approx 1$, $\Omega_P/2\pi \approx 0.5$ GHz, $T_T^* \leqslant 30$ mK, $k^2 \cdot Q \cdot \beta_L \leqslant 1$, this gives $(\varepsilon_V)_T \approx \xi \times 10^{-33}$ J Hz^{-1}. Here, ξ is a coefficient of the order of 1.

The achievement of the sensitivity approaching the quantum limit $\delta\varepsilon \cdot \delta t \approx h$ is hindered by the noises of the resonator and amplifier. These contributions to the total sensitivity of the RF SQUID can be significantly reduced [19–21] using the regime $k^2 \cdot Q \cdot \beta_L \gg 1$, $\beta_L \leqslant 1$, and choosing the operating point in the vicinity of the 'vertical' regions on the AFC, see figure 6. It is clear that if the operating point is chosen close enough to such a 'vertical' region, then a small change in the external flux (signal) will cause a significant change in the amplitude and the phase of oscillations in the resonator. Near the 'vertical' region, the flux-amplitude and flux-phase transfer coefficients can be made much larger than the value of equation (3). This condition, most probably, has been realized so far only in [21].

By varying the detuning and the pump amplitude near the 'vertical' region, we managed to obtain $\eta_{a,\theta} \approx 4 \times 10^{12}$ V Wb^{-1} in an RF SQUID with 30 MHz pump frequency. It follows from the analysis of the RF SQUID sensitivity [12, 19–21] that in this case the optimal operating point is near the first maximum of the Bessel function $J_1(a)$, at $a = 1.8$. With such transfer coefficients, the noise contribution of the

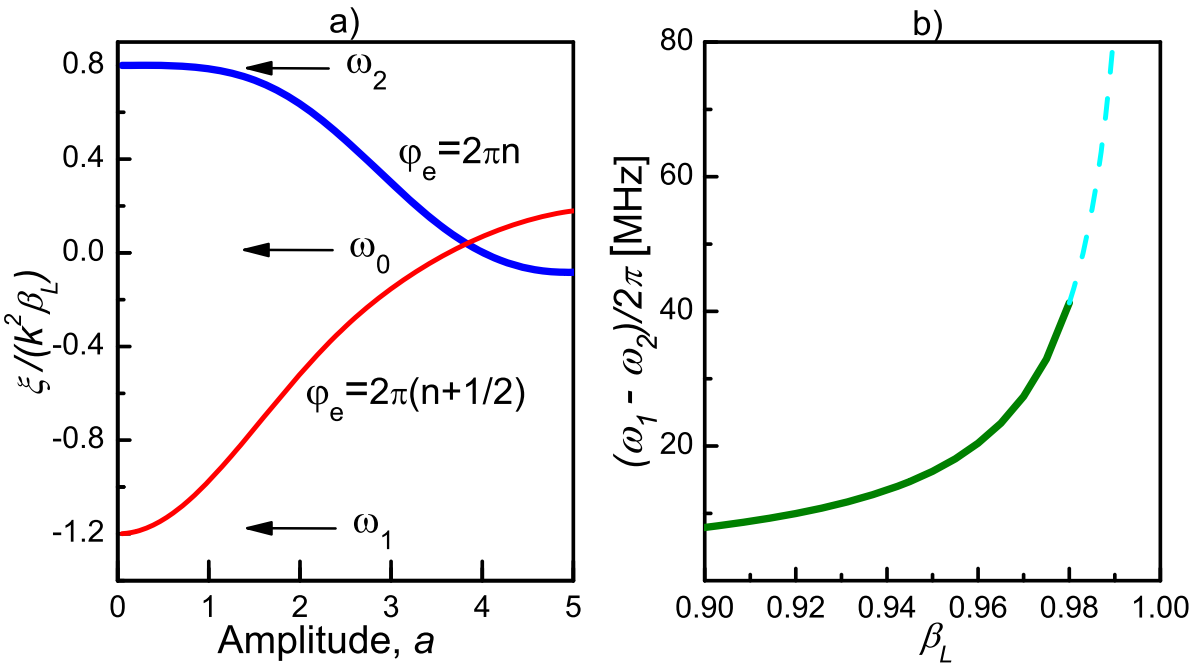

Figure 7. (a) Numerical simulation using (11). Normalized detuning $\xi/(k^2\cdot\beta_{\rm L})$ (resonant frequency) of the RF SQUID with $\beta_{\rm L}=0.25$ vs. pumping amplitude a for two values of the external magnetic flux. Extreme resonator frequencies are denoted by ω_1,ω_2 (b). The extreme frequency difference $(\omega_1-\omega_2)/2\pi$ as a function of $\beta_{\rm L}$ for RF SQUID calculated using (12) t with parameters $\omega_0/2\pi=\Omega_{\rm P}/2\pi=0.5$ GHz, $k^2\cdot Q=1$, $Q=300$.

amplifier $\delta\varepsilon_{\rm A}\sim|\eta_{a,\theta}|^{-2}$ becomes negligible. However, with an increase in the transfer coefficients near one of these points, the input frequency band decreases as $|\eta_{a,\theta}|^{-1}$ [20, 21]. Moreover, the back action of the RF SQUID onto the qubit also increases. The contribution of the resonator noise given by equation (8) in comparison with the intrinsic noise of the interferometer (equation (7)) can be neglected only if this rather complicated condition is satisfied

$$\gamma=k^2\cdot Q\cdot\beta_{\rm L}\frac{\Omega_{\rm P}}{\omega_{\rm C}}\gg\frac{T_{\rm T}^*}{T} \tag{9}$$

Since $\Omega_{\rm P}$ is given by equation (6), then inequality (9) can be satisfied by increasing $Q,\beta_{\rm L}$ and (or) the coupling coefficient k^2 with the interferometer. With this sensitivity improving scenario, it is necessary to take into account that the input bandwidth of the photon counter decreases with the quality factor rise, $\Delta f\sim Q^{-1}$.

To obtain sensitivity at the interferometer intrinsic noise level $\delta\varepsilon\cdot\delta t\approx h$, one must meet condition (9), increase the pump frequency to $\Omega_{\rm P}>(E_1-E_0)/\hbar$, use high enough normal junction resistance $R\approx100$ Ohm to maintain the adiabatic approximation $q=\Omega_{\rm P}\cdot L/R\ll1$ and finite pumping amplitudes $a\approx1.8$. Of course, this pump amplitude is smaller than in the hysteretic mode, but it can also lead to unwanted counter excitations.

4. RF SQUID in the regime $\beta_{\rm L}\leqslant1$, $k^2\cdot Q\cdot\beta_{\rm L}\leqslant1$ at low pumping amplitudes

In any dispersive method for measuring a quantum system state, one of the main requirements is to minimize the amplitude of the electromagnetic field in the parametric resonator. From this point of view, let us consider the frequency (phase) characteristics of the RF SQUID in non-hysteretic ($\beta_{\rm L}\leqslant1$) adiabatic ($q\ll1$) mode under conditions $k^2\cdot Q\cdot\beta_{\rm L}\leqslant1$, $a\ll1$. In this limit, there are no vertical regions (break points) in the frequency response curves, and the amplitude flux-voltage transfer coefficient η_a approaches the value of equation (3) for $\beta_{\rm L}\leqslant1$. Using the equations from ,[22] for damping $2\delta(a,\varphi_{\rm e},\beta_{\rm L})$ and effective detuning $2\xi(a,\varphi_{\rm e},\beta_{\rm L})$, we can analyze these quantities at small amplitudes of the electromagnetic field in the parametric resonator of the RF SQUID. In the limit $a\ll1$, $q\ll1$, leaving only terms proportional to $\beta_{\rm L},\beta_{\rm L}^2$ for damping and detuning in the original equations, we obtain

$$2\delta(a,\varphi_{\rm e},\beta_{\rm L})\cong Q^{-1} \tag{10}$$

$$2\xi(a,\varphi_{\rm e},\beta_{\rm L})\approx2\xi_0-k^2\cdot\beta_{\rm L}\left[\frac{2\cdot J_1(a)}{a}\cos(\varphi_{\rm e})-\beta_{\rm L}\frac{J_1(2a)}{a}\cos(2\varphi_{\rm e})\right]. \tag{11}$$

At low SQUID excitation amplitudes, the damping of equation (10) is practically independent of $\varphi_{\rm e}$. It follows that, at small amplitudes, the AFC have the same form as for a linear resonator with a constant quality factor. All nonlinear effects are associated with detuning given by equation (11), which is a Φ_0-periodic function of the external magnetic flux. Figure 7(a) shows the numerical simulation using (11) for the normalized dependences of the resonant frequency of the parametric resonator on the oscillation amplitude for two values of

the magnetic flux φ_e. In the limit $a \to 0$, all signal characteristics of the RF SQUID are confined in the range between two extreme frequencies ω_1, ω_2 and do not depend on the oscillation amplitude.

$$\frac{\omega_1 - \omega_2}{\omega_0} = k^2 \cdot \frac{\beta_L}{1 - \beta_L^2}. \tag{12}$$

Expression (12) is valid for any $\beta_L < 1$. Figure 7(b) shows the numerical simulations using (12) for the extreme frequency difference $(\omega_1 - \omega_2)/2\pi$ as a function of β_L. In the region $\beta_L = 0.95 \pm 0.05$, the range of frequency variations of the parametric resonator and the corresponding transfer coefficients increase sharply. For quantum measurements, it is important that the high sensitivity of the RF SQUID, limited by the resonator noise, can be obtained in the region of extremely small driving amplitudes $a = 2\pi \cdot \Phi_a \Phi_0^{-1} \ll 1$, formally at $a \to 0$.

So, by choosing the pump frequency far from the resonance of the two-level system $\Omega_P \ll (E_1 - E_0)/\hbar$ and making the amplitude of the electromagnetic field in the cavity of the parametric converter extremely small (slightly larger than the natural thermal fluctuations of the resonator), one can significantly suppress the back-action effect of the non-hysteretic RF SQUID readout on the flux qubit in the MW single photon counter.

5. Concluding remarks

Three scenarios of WCMs of states of the flux qubit in a single photon counter by RF SQUIDs are considered. The proper choice of RF SQUID parameters is dictated by the following. The RF SQUID loop inductance of $L \approx 200$ pH is determined to match the flux qubit inductance. The excitation frequency $\Omega_P/2\pi \approx 500$ MHz was chosen so that it is much less than the resonant frequency of the qubit $(E_1 - E_0)/\hbar$, and does not coincide with the multiphoton absorption peaks of the qubit as a two-level artificial atom. The shunt resistance of the Josephson SIS junction $R \approx 10$ Ohm is given by the existing technology [23]. With such a shunt resistance, the parameter that determines nonadiabatic phenomena and losses in the interferometer is quite small, $q = \Omega_P \cdot L/R \approx 0.06$. This value can be reduced by an order of magnitude by using other types of Josephson junctions [20, 23, 24].

With these parameters, the magnetic flux sensitivity of the RF SQUID to a flux change in its input loop at $T \leqslant 30$ mK in the hysteretic regime is $\delta\Phi_{min} \approx 7 \times 10^{-7}\Phi_0\sqrt{\text{Hz}}^{-1}$) with the maximum energy sensitivity $\delta\varepsilon_V \approx 10^{-32}$ J Hz^{-1}. However, using a RF SQUID in this mode in quantum measurements is limited by hysteresis losses and, most importantly, by the need to use large resonator pump amplitudes. In the non-hysteretic adiabatic regime, the RF SQUID is a sensitive parametric up-converter. As noted above (figure 7(b)), its transfer coefficient and sensitivity rapidly increase at $\beta_L \to 1$, $a \ll 1$. To implement the necessary condition $\beta_L = 0.95 \pm 0.05$, with $L = 200$ pH, the critical current of the RF SQUID Josephson junction must be in the interval $I_c = 1.5$–$1.65\,\mu$A. In this case, the McCumber parameter $\beta_C = 2\pi \cdot R^2 \cdot I_c \cdot C/\Phi_0 \approx 0.1$ and the influence of thermal fluctuations is small $2\pi k_B T/(I_c \cdot \Phi_0) \leqslant 10^{-3}$ at a temperature $T \approx 10$ mK. The maximum speed of the RF SQUID is determined by the resonator bandwidth, which is about 1 MHz at the resonator quality factor $Q \approx 300$–400. From the point of view of quantum measurements, the main advantages of the non-hysteretic adiabatic regime of the RF SQUID are: (a) extremely low amplitudes of the electromagnetic field in the resonator, which means very small back-action effect of the RF SQUID on the qubit; (b) sufficiently high transfer coefficients and sensitivity to the input signal $\delta\Phi_{min} \approx 2.2 \times 10^{-7}\Phi_0\sqrt{\text{Hz}}^{-1}$, $\delta\varepsilon_V \approx 10^{-33}$ J Hz^{-1}. This estimation of the RF SQUID sensitivity in the non-hysteretic adiabatic regime is still an order of magnitude from the quantum limit, which justifies the use of the classical theory at the 10 mK temperature range in our work.

Advances in the technology of manufacturing high-quality Josephson junctions with small area and high critical current densities have made it possible to obtain a sensitivity for DC SQUIDs approaching the quantum limit: $\delta\varepsilon_V \delta t \approx h$, and hence enabled their application in quantum measurements. New experimental methods of the 'dispersive readout' type for measuring the state of superconducting qubits using DC SQUIDs have been proposed and tested [25–28]. This dispersive readout technique is very close to that considered in our paper. In many instances, readout back-action decreases with lowering readout pumping amplitude. The signal detection channel considered in this work and based on an almost ideal parametric transducer, combines minimal back action with high sensitivity and speed, and are potentially applicable to continuous monitoring of the flux-qubit-based single MW photon counter.

The experiments with RF SQUIDs at temperatures 2 K and 4.2 K were carried out using a network analyzer (sweep generator) similar to [29] at the Institute for Low Temperature Physics and Engineering and the data analysis was carried out by the authors jointly.

Data availability statement

All data that support the findings of this study are included within the article (and any supplementary files).

Acknowledgments

We acknowledge the help of Alexander Kordyuk and useful discussions with Oleg Turutanov and Alexey Korolev. This work was carried out within the framework of Project G5796 funded by the NATO Science for Peace and Security Programme and Project No. 0121U110046 funded by the Applied Research Programme of the Ministry of Education and Science of Ukraine.

ORCID iDs

V I Shnyrkov https://orcid.org/0000-0001-7492-1302
A P Shapovalov https://orcid.org/0000-0002-2181-9416
V Yu Lyakhno https://orcid.org/0000-0002-2543-1240

A O Dumik https://orcid.org/0000-0002-3867-5260
A A Kalenyuk https://orcid.org/0000-0002-7212-434X
P Febvre https://orcid.org/0000-0002-9302-0419

References

[1] Chen Y-F, Hover D, Sendelbach S, Maurer L, Merkel S T, Pritchett E J, Wilhelm F K and McDermott R 2011 Microwave photon counter based on Josephson junctions *Phys. Rev. Lett.* **107** 217401
[2] Inomata K, Lin Z, Koshino K, Oliver W D, Tsai J-S, Yamamoto T and Nakamura Y 2016 Single microwave-photon detector using an artificial Λ-type three-level system *Nat. Commun.* **7** 12303
[3] Gu X, Kockum A F, Miranowicz A, Liu Y and Nori F 2017 Microwave photonics with superconducting quantum circuits *Phys. Rep.* **718–719** 1–102
[4] Eisaman M D, Fan J, Migdall A and Polyakov S V 2011 Invited review article: single-photon sources and detectors *Rev. Sci. Instrum.* **82** 071101
[5] Pechal M, Huthmacher L, Eichler C, Zeytinoglu S, Abdumalikov A A Jr, Berger S, Wallraff A and Filipp S 2014 Microwave-controlled generation of shaped single photons in circuit quantum electrodynamics *Phys. Rev.* X **4** 041010
[6] Peng Z H, de Graaf S E, Tsai J S and Astafiev O V 2016 Tuneable on-demand single-photon source in the microwave range *Nat. Commun.* **7** 12588
[7] Shnyrkov V I, Yangcao W, Soroka A A, Turutanov O G and Lyakhno V Yu 2018 Frequency-tuned microwave photon counter based on a superconductive quantum interferometer *Low Temp. Phys.* **44** 213–20
[8] Soroka A A and Shnyrkov V I 2013 A tunable coupler with ScS quantum point contact to mediate strong interaction between flux qubits *J. Low Temp. Phys.* **172** 212–25
[9] Ketchen M 1981 DC SQUIDs 1980: the state of the art *IEEE Trans. Magn.* **17** 387–94
[10] Clarke J and Braginski A I 2004 *The Squid Handbook, Fundamentals and Technology of Squids and Squid Systems* (Weinheim: Wiley-VCH Verlag GmbH Co. KGaA)
[11] Friedman J R, Patel V, Chen W, Tolpygo S K and Lukens J E 2000 Quantum superposition of distinct macroscopic states *Nature* **406** 43
[12] Shnyrkov V I and Tsoi G M 1992 *Principles and Applications of Superconducting Quantum Interference Devices* ed A Barone (Singapore: World Scientific) p 77
[13] Korolev A M, Shnyrkov V I and Shulga V M 2011 Ultra-high frequency ultra-low DC power consumption HEMT amplifier for quantum measurements in milliKelvin temperature range *Rev. Sci. Instrum.* **82** 016101
[14] Korolev A M, Shulga V M, Turutanov O G and Shnyrkov V I 2015 A wideband radio-frequency amplifier for investigations at temperatures from 300 to 0.1 K *Instrum. Exp. Tech.* **58** 478–82
[15] Korolev A M, Shulga V M, Gritsenko I A and Sheshin G A 2015 PHEMT as a circuit element for high impedance nanopower amplifiers for ultra-low temperatures application *Cryogenics* **67** 31
[16] Mück M 1992 A readout system for 3-GHz RF SQUIDs *Rev. Sci. Instrum.* **63** 2268–73
[17] Long A P, Prance R J, Clark T D, Mutton J E, Potts M W, Widom A and Goodall F 1980 Quantum limited AC biased SQUID magnetometer *Superconducting Quantum Interference Devices and Their Applications* ed H D Hahlbohm and H Lubbig (Berlin: de Gruyter) pp 207–11
[18] Kurkijarvi J 1972 Intrinsic fluctuations in a superconducting ring closed with a Josepshon junction *Phys. Rev.* B **6** 832–5
[19] Likharev K K 1986 *Dynamics of Josephson Junctions and Circuits* (New York: Gordon and Breach Science Publishers)
[20] Ryhunen T, Seppa H, Illimoniemi R and Knuutila J 1989 *J. Low Temp. Phys.* **76** 287–386
[21] Dmitrenko I M, Tsoi G M, Shnyrkov V I and Kartsovnik V V 1982 RF SQUID in the nonhysteretic regime with $k^2 \cdot Q \cdot l > 1$ *J. Low Temp. Phys.* **49** 417–33
[22] Jackel L D and Buhrman R A 1975 Noise in the RF SQUID *J. Low Temp. Phys.* **19** 201–46
[23] Shapovalov A P, Shaternik V E, Turutanov O G, Lyakhno V Yu and Shnyrkov V I 2019 On the possibility of faster detection of magnetic flux changes in a single-photon counter by RF SQUID with MoRe-Si(W)-MoRe junction *Low Temp. Phys.* **45** 776–86
[24] Walsh E D, Efetov D K, Lee G-H, Heuck M, Crossno J, Ohki T A, Kim P, Englund D and Fong K C 2017 Graphene-based Josephson junction single photon detector *Phys. Rev. Appl.* **8** 024022
[25] John C *et al* 2002 Quiet readout of superconducting flux states *Phys. Scr.* **T102** 173–7
[26] Wallraff A, Schuster D I, Blais A, Frunzio L, Majer J, Devoret M H, Girvin S M and Schoelkopf R J 2005 Approaching unit visibility for control of a superconducting qubit with dispersive readout *Phys. Rev. Lett.* **95** 060501
[27] Lupascu A, Driessen E F C, Roschier L, Harmans C J P M and Mooij J E 2006 Dispersive readout of a superconducting flux qubit using a nonlinear resonator *Phys. Rev. Lett.* **96** 127003
[28] Johnson J E, Hoskinson E M, Macklin C, Slichter D H, Siddiqi I and Clarke J 2011 Dispersive readout of a flux qubit at the single-photon level *Phys. Rev.* B **84** 220503
[29] Shnyrkov V I, Khlus V A and Tsoi G M 1980 On quantum interference in a superconducting ring closed by a weak link *J. Low Temp. Phys.* **39** 477–96